Siu-Kui Au[1], James M.W. Brownjohn[2], Binbin Li[3], Alison Raby[4]

Abstract

Close modes are much more difficult to identify than well-separated modes and their identification (ID) results often have significantly larger uncertainty or variability. The situation becomes even more challenging in operational modal analysis (OMA), which is currently the most economically viable means for obtaining in-situ dynamic properties of large civil structures and where ID

spatial (mode shape) properties by matrix-decomposition of the PSD matrix

loss of information); and probabilistic information in data has been processed in a consistent manner following rigorously Bayes' rules.

Figure 1 Schematic diagram showing the theoretical singular value spectrum of ambient data on a resonance band with two close modes

In the above context, we have obtained analytical expressions for the ‘remaining’, i.e., ID uncertainty,

uncertaintyu

$$\frac{2}{2}\ \frac{1}{i}\ (\ 2)\ \frac{1}{1\ \ \frac{2}{2}|\ |^2}$$

s/n effect — Dim. to MSS

analogous to well-separated modes

coherence effect

See Figure 6 later for a geometric interpretation. The definitions of the above parameters are motivated from the analytical expressions of the c.o.v.s, i.e., they carry fundamental significance instead of being empirically defined. See Table 7 of the companion paper for a summary.

Compared to mode shapes, the ID uncertainty of frequencies and damping ratios for close modes are affected in a less systematic manner by disparity. They are only correlated with Type 2 mode shape uncertainty. We show that the c.o.v. of natural frequencies σ_{f_i} and damping ratios σ_{ζ_i} are given by (see Section 6.5 of companion paper for proof)

$$\sigma_{f_i}^2 \sim \underbrace{\frac{\zeta_i}{2 S_i N_{ci}}}_{\text{same for well-separated modes}} \underbrace{u \; Q_{f_i}}_{\text{coherence effect}}, \tag{8}$$

$$\sigma_{\zeta_i}^2 \sim \underbrace{\frac{1}{2 S_i N_{ci}}}_{\text{same for well-separated modes}} \underbrace{u \; Q_{\zeta_i}}_{\text{coherence effect}} \tag{9}$$

where Q_{f_i} and Q_{ζ_i} are coherence factors given by:

$$Q_{f_i} \quad \frac{1 \;|\; A|^2}{1 \;\; q_2^2 \,|\, A|^4} \quad \frac{|\; A|^2 \, R_{f_i}}{(1 \;\; q_2^2 \,|\, A|^2)(1 \;\; q_1^2 \,|\, A|^4)(1 \;\; q_2^2 \,|\, A|^4)} \tag{10}$$

$$Q_{\zeta_i} \quad \frac{1 \;|\; A|^2}{1 \;\; q_2^2 \,|\, A|^4} \quad \frac{|\; A|^2 \, R_{\zeta_i}}{(1 \;\; q_2^2 \,|\, A|^2)(1 \;\; q_1^2 \,|\, A|^4)(1 \;\; q_2^2 \,|\, A|^4)} \tag{11}$$

R_{f_i} and R_{ζ_i} are factors that depend on the phase angles $/$, l and $/_i \quad \tan^{1} c_i / e_i$:

$$\begin{aligned} R_{f_i} \quad & (1 \;\; q_2^2 \,|\, A|^2)^2 \cos^2(/ \;\; s_i /_i) \quad (1 \;|\; A|^2)^2 q_2^2 \sin^2(/ \;\; s_i /_i \;\; l) \\ & 2 q_1 q_2 \,|\, A|^2 (1 \;\; q_2^2 \,|\, A|^2)(1 \;|\; A|^2) \cos(/ \;\; s_i /_i) \sin(/ \;\; s_i /_i \;\; l) \end{aligned} \tag{12}$$

$$\begin{aligned} R_{\zeta_i} \quad & (1 \;\; q_2^2 \,|\, A|^2)^2 \sin^2(/ \;\; s_i /_i) \quad (1 \;|\; A|^2)^2 q_2^2 \cos^2(/ \;\; s_i /_i \;\; l) \\ & 2 q_1 q_2 \,|\, A|^2 (1 \;\; q_2^2 \,|\, A|^2)(1 \;|\; A|^2) \sin(/ \;\; s_i /_i) \cos(/ \;\; s_i /_i \;\; l) \end{aligned} \tag{13}$$

where $s_1 \quad 1$ and $s_2 \quad 1$. Note that swapping the sines and cosines in R_{f_i} gives R_{ζ_i} .

As uncertainty law, (1), (8) and (9) give the leading order value of the remaining uncertainty about the modal properties identified from ambient vibration data under test configuration and environment quantified by various parameters in the formulae.

For instructional purpose it is useful to review the uncertainty law for well-separated modes so that we can see what difference the close mode problem makes and what factors matter. For well-separated modes identified with a wide resonance band, the c.o.v.s are given by [39]

$$\sigma_{f_i}^2 \sim \frac{1}{2\beta_i f_i N_{ci}} \left(\frac{1}{4\zeta_i^2} + (n-1)\right) \qquad \sigma_{\zeta_i}^2 \sim \frac{\zeta_i}{2\beta_i f_i N_{ci}} \qquad \sigma_{\phi_{ji}}^2 \sim \frac{1}{2\beta_i f_i N_{ci}} \tag{15}$$

The c.o.v.s in (2), (3), (8) and (9) have been written as the values for well-separated modes multiplied by various effects brought by close modes. The c.o.v.s of frequencies and damping ratios are only affected by modal force coherence ρ

or when the two modes get closer (smaller d_i). In Sections 3.3 to 3.5 to follow, we discuss systematically the effect of modal disparity (i.e., how modes differ) and modal force coherence.

One basic question in the study of close modes is

'How close is close?'

Equation (3) reveals that for ID uncertainty the fundamental definition that measures the difference of modes in an overall sense is $d_i \quad \sqrt{c_i^2 \quad e_i^2}$, where $e_i \quad (f_j \quad f_i)/f_i \,]_i$ and

i j j i i i i

Figure 4 Dynamic amplification factors of two modes with different frequency disparities e_1 of 0.5 (very close), 1 (close), 5 (separated) and 10 (well-separated). The two modes have the same damping (1%) and so $d_i = e_i$

As a note, it may appear from (3) that decreasing damping increases G_{ij}

(11) also depend on the phase angles l , $/$ and $/_i$ through the factors R_{f_i} and R_{J_i} in (12) and (13). Such dependence is trigonometric in nature and is of less significance than those on q_2 and $|\ A|$. It is shown in Section 11 (appendix) that

$$0\ dR_{x_i}\ \ d(1\ \ q_2^2|\ A|^4)[1\ \ q_2^2|\ A|^2\ \ q_2^2(1\ \ |\ A|^2)] \qquad x\ \ f\ ,\ J \qquad (19)$$

Substituting into (10) or (11), |

Figure 5 Lower bound ($1 - |A|^2$) and upper bound ($(1 - |A|^2)^{-1}$) of coherence factors Q_{f_i} and Q_{f_i} in (21); Q_{3_i} share the same upper bound but it is bounded below by 1, see (18).

q_i

The effect of disparity parameters (e_i, c_i) on the modal entangling factors q_i is obscured by their relationship with another two entangling factors g_i in (6), on which q_i in (5) depends. Generally, increasing disparity reduces the magnitude of q_i and hence the influence of coherence, which is intuitively correct. It can be shown by direct algebra that the following identity holds:

$$(g_1 - r)^2 - g_2^2 - r^2 \qquad r - \frac{1}{\sqrt{(2 - c_1)(2 - c_2)}} \tag{22}$$

igure

Figure 6 Geometric interpretation of the effect of disparity on modal entangling factors g_1, g_2 and q_2 in (5). Note that $_1$ $_2 \sin(2$ $)$

where - $[\Psi_1, \Psi_2]$ (n u2 real partial mode shape matrix) and S_k $[p_{1k}, p_{2k}]^T$ (2 u1 complex vector of modal forces) is the scaled FFT of modal forces and $_k$ is the scaled FFT of noise.

length can be significantly longer than that for well-separated modes when disparity is small (even for noiseless data). This governs the achievable identification precision of close modes. It should be noted that the issue of disparity discussed here is related to the temporal/frequency rather than spatial aspect of response/data. It does not have a direct linkage with observability that is often discussed in the system identification literature.

The results in Section 2 assume that the resonance band for modal ID is sufficiently wide, in the sense that $N!\,!1$ and $N!\,!\,e_q$. In the development of theory it was found necessary to introduce this assumption in order to obtain rigorously the closed form asymptotic expressions for c.o.v.s with reasonable simplicity as presented in the section. On other hand, the expressions capture only the leading order of the c.o.v.s which turn out to be independent of the noise PSD S_e and hence s/n ratio, except for Type 1 mode shape uncertainty which is nevertheless negligible for high s/n ratio. Finite bandwidth and s/n ratio encountered in reality do make a difference to ID uncertainty especiallysnth-1.3 (p)7.3 (t)447 (o)arpno

In Table 1,

$$N \quad \frac{\text{bandwidth(Hz)}}{2 f \, J} \qquad\qquad J\mathbb{C} \quad \frac{S}{4 S_{e} J^{2}} (1 \quad \mathcal{U}^{2})(1 \mid A\dagger^{2}) \qquad (26)$$

$$J_{c}$$

Check that these mode shapes have unit norm and their MAC is $\mathcal{L}$

			| A| on 0-1 and / on 0 - 2 S Resulting N= 10 – 20+, s/n ratio = 1000 – 10^4+ Figure 10
Lab model	600 sec/set x 54 set = 3 h at 256Hz	4 DOFs, xy at two corners on long side of top floor	3-storey shear frame, 5kg per floor, wide bandwidth, low to high s/n ratio with electric fan at different distances N 2 – 20, s/n ratio = 10 – 10^4+ Figure 11 and Figure 12
Building B in [12]	30 min./set x 72 set = 36 h at 50Hz	3 DOFs, xyz near core on roof; see Fig@,e0G&3 [12][12]6 CDnmrg@12]2'bG	

Figure 9 Some structures considered in the study

The synthetic data features a moderately high s/n ratio (>1000), wide band ($\Delta f \approx 10$) and long data (about 1000 natural periods in each set). One hundred data sets with different modal properties are randomly generated to cover a variety of scenarios. Figure 10(a)-(c) show the c.o.v.s of frequencies, damping ratios and mode shapes. Recall that the mode shape c.o.v. is defined as the square root sum of eigenvalues of the mode shape posterior covariance matrix. For small value, it can be interpreted as the expected hyper-angle between the uncertain mode shape and its MPV. The x-axis shows the values calculated by Bayesian modal ID algorithm (BAYOMA) [28] for each data set. This is the value one uses in applications for assessing ID uncertainty conditional on the particular data set when it is available; but the point-wise value does not explain the calculated uncertainty. In BAYOMA, the most probable value (MPV) of modal parameters is first calculated by minimising the negative log of the likelihood function (NLLF). The posterior covariance matrix of modal parameters is then calculated as the inverse of the Hessian of NLLF evaluated at the MPV. Each diagonal entry of this matrix gives the corresponding posterior variance of the parameter, which subsequently gives the c.o.v. (= square root of variance/MPV) that is plotted on the x-axis.

In Figure 10(a)-(c), the y-axis shows the uncertainty law values developed based on different

uncertainty. The red circles show the values based on the inverse of the exact Fisher Information Matrix (FIM); see Section 3.1 and (14). Being a theoretical ensemble average over long data in hypothetical repeated experiments distributed according to the same likelihood function of BAYOMA, the exact FIM (or uncertainty law) value does not depend on the particular data set used but rather the 'true' modal properties (which is assumed to exist). Although the latter is known in this synthetic data example, it is not known (in fact, does not exist) in general applications with experimental data. To be consistent with the general context, when calculating the exact FIM (or uncertainty law) value the true parameter value is substituted by the most probable value (MPV) calculated by BAYOMA based on the particular data set. Statistically significant deviation of the exact FIM values (red circles) from the 1:1 line is an indication of modelling error for that particular data set. For its semi-analytical nature, the exact FIM can be considered as one step towards explaining ID uncertainty. Nevertheless its implicit nature (e.g., still in terms of matrices) does not yet allow direct insights to be developed. This ultimate goal is addressed by the uncertainty law developed, i.e., wide band expressions ((1), (8) and (9)) modified by the factors in Table 1 to account for finite bandwidth and s/n ratio. Their values are shown as crosses ('x') in Figure 10(a)-(c). They represent the best effort of this work to explain the ID uncertainty of close modes. They agree with the red circles, effectively verifying the mathematical correctness of the wide band law.

As a remark, if the data used is long and it is indeed distributed as the same likelihood function as in BAYOMA/FIM, i.e., no modelling error (as is possible for synthetic data here), the BAYOMA value (x-axis) will theoretically converge (in a statistical sense) to the exact FIM value (y-axis, red circle). In this sense the exact FIM value is the closest analytical value one can get to match the BAYOMA value; see [45] for a further discussion. However, this convergence is only a theoretical statement which can at best be expected from synthetic data because no model is perfect for experimental data. This aspect of convergence is only relevant in the verification of mathematical correctness (at the research stage) of the exact FIM or uncertainty law where synthetic data must be used. It is irrelevant to the intended application of uncertainty law, however, which is to understand and manage ID uncertainty for planning tests where no data is available.

Figure 10(e) shows $\sqrt{Q_{ji}}$ in (11), which is the amplification of damping c.o.v. due to modal force coherence γ. The amplification depends on $|\rho|$ and other parameters but it is bounded between $1 - |\rho|^2$ and $(1 - |\rho|^2)^{-1}$ as in (21). This is demonstrated in the plot. Finally, Figure 10(f) shows the values of $|\rho|$ and ζ (MAC) among the data sets. For the synthetic data sets here they are distributed uniformly merely because of the way they are generated. For the laboratory and field cases later they reflect statistics in the corresponding situations.

We now discuss the results of the laboratory and field data in a collective manner w.r.t. different aspects. Figure 11, Figure 13, Figure 15, Figure 17 and Figure 19 show the spectra (PSD and SV) of a typical data set in each case. The results analogous to Figure 10 are summarised in Figure 12, Figure 14, Figure 16, Figure 18 and Figure 20.

The cases collectively cover low to high s/n ratios, from a few tens to over ten thousand. The laboratory shear frame is intended to provide an experimental case under controlled environment. Rugeley Chimney provides a case with obvious violation of modelling error, i.e., non-classical damping due to tuned mass damper (TMD). Modal ID of the field structures has been studied previously; see references in the first column of Table 2. The current investigation provides an opportunity to understand their ID uncertainties. The tall building, lighthouse and chimney have close fundamental modes that govern their vibration response, giving compelling reasons for their proper identification and understanding. The lighthouse data is unconventional; obtaining it is a challenge in itself.

On the verification side, in the plots (a)-(c) of Figure 12, Figure 14, Figure 16, Figure 18 and Figure 20, the crosses roughly match with the red circles, suggesting that the proposed formulae (wide band expressions with empirical factors) can give a good match with what can be best achieved (exact FIM). Outliers do exist, e.g., for laboratory frame (one point in Figure 12(c)). The amount of scattering in the crosses and circles about the 1:1 line is similar in all cases except for Rugeley Chimney, which is a special case with modelling error to be discussed later. Similar to the case of synthetic data, the green dots (well-separated modes law) in plot (c) fall below the 1:1 line by orders of magnitude, showing that they fail to explain the ID uncertainty of mode shapes of close modes. They perfor[oeron(th-0.0- ((f)2.6 er)3.2 eqh)5.3 u

Table 3 gives a summary of the statistics of the identified (MPV) damping ratio, disparity, coherence and MAC between the two modes in each band. It can be examined together with plots (d)-(f) in Figure 12, Figure 14, Figure 16, Figure 18 and Figure 20.

Table 3 Summary of statistics for experimental cases. Some low values of disparity and high values of coherence and MAC are highlighted in bold

		Damping ζ_i			Disparity d_i			Coherence γ^2			MAC ϕ C /Artifact Reference114 >>BDC Qq375.24 37 92.56 0.481 reC		
Case	Band	Min.	Mean	Max.	Min.	Mean	Max.	Min.	Mean	Max.	Min.	Mean	Max.
Lab frame	1	0.5%	0.7%	1.1%	1.1	2.2	3.8	0.03	0.17	0.38	0.00	0.07	0.23
(Figure 10)	2	0.6%	0.8%	1.0%	1.3	2.0	2.7	0.09	0.23	0.45	0.00	0.21	0.51
	3	0.4%	0.9%	2.0%	1.3	3.7	6.9	0.01	0.20	0.36	0.01	0.11	0.26
Tall building	1	0.3%	1.4%	3.9%	**0.3**	2.1	10	0.03	0.31	**0.82**	0.00	0.24	**0.85**

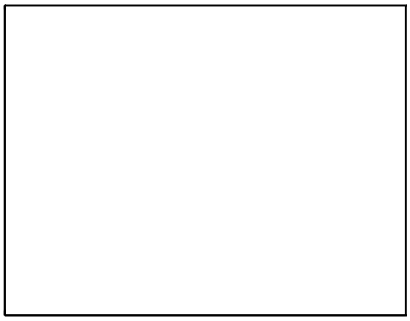

Figure 11 PSD and SV spectra of a typical data set, laboratory shear frame

Figure 12 Summary of results, Laboratory shear frame. Same legend as Figure 10

Figure 13 PSD and SV spectra of a typical data set, tall building

Figure 14 Summary of results, tall building. Same legend as Figure 10

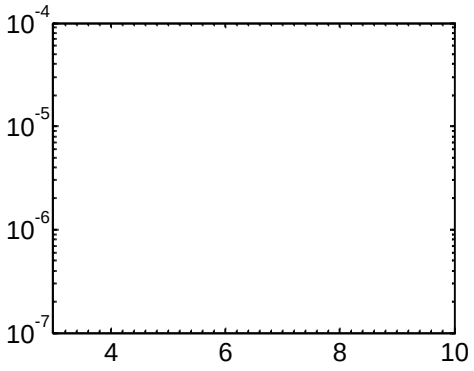

Figure 15 PSD and SV spectra of a typical data set, Eddystone lighthouse

Figure 16 Summary of results, Eddystone lighthouse. Same legend as Figure 10

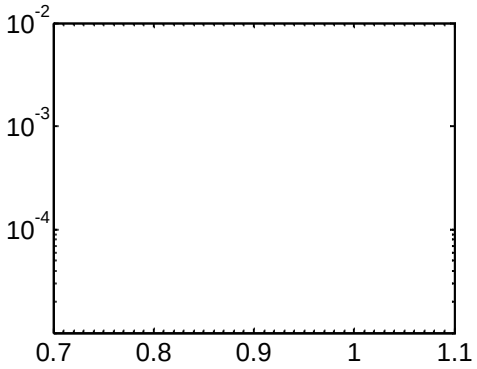

Figure 17 PSD and SV of a typical data set, Jiangyin Yangtze River Bridge

Figure 18 Summary of results, Jiangyin Yangtze River Bridge. Same legend as Figure 10

Well-separated modes are conventional subjects in modal ID. A logical way to think about the implications of uncertainty law of close modes developed in this work is to see what concepts or requirements need to be adjusted/introduced beyond those already in place for well-separated modes [39]. This is how the c.o.v.s of frequencies and damping ratios in (8) and (9) have been written. Close modes bring in the coherence factors Q_{f_i} and Q_{ζ_i} in (10) and (11). It is more useful to think of the coherence factors in terms of the bounds in (21); see also Figure 5. Further correction to capture the effect of bandwidth and s/n ratio is needed. This can be done using the empirical factors in Table 1, where the modal s/n ratio γ_i^2 is equal to the old one for well-separated modes (γ_i^2) discounted by $(1 + R_i^2)$ and $(1 - \theta^2)$.

Close modes bring additional uncertain dimensions to mode shapes and this overturns our intuition about the governing uncertainty accumulated for well-separated modes. Mode shape uncertainty is no longer negligible. It can even render the problem unidentifiable. For well-separated modes it is always orthogonal to the identified mode shape direction (Type 1, see (2) and Figure 2) and is negligible for high s/n ratio. For close modes, Type 1 uncertainty remains to be negligible for high s/n ratio, but the additional non-vanishing uncertainty (Type 2, see (3)) smearing between mode shapes is of the same order of magnitude as or even larger than damping uncertainty. Based on (3), one can think of the mode shape c.o.v. (Type 2) as being equal to the damping c.o.v. amplified by the effects of disparities ($1/d_i$ and $\sqrt{S_{jj}/S_{ii}}$), MAC ($\sqrt{1-\theta}$) and coherence ($\sqrt{Q_{3i}}$). It is useful to think of Q_{3i} in terms of its upper bound, which coincides with those of frequency and damping in Figure 5. Accordingly, doubling the c.o.v. will account for the effect of coherence in most cases.

Uncertainty law for well-separated modes was developed in [39] to allow one to manage quantitatively the ID uncertainty. In this case damping uncertainty is the governing factor and its c.o.v. is given by

$$\delta_\zeta \approx \frac{1}{\sqrt{2\zeta N_c}} \quad \text{(well-separated mode)} \qquad (29)$$

where ζ is the damping ratio (mode number omitted), N_c is the dimensionless duration as a multiple of natural periods, e.g., a duration of 100 sec for a 2Hz mode gives $N_c = 100 \times 2 = 200$;

A_J and A_Λ account for finite s/n ratio and bandwidth, respectively, and are calculated according to Table 1 with (omitting index i) J_0 replaced by $J_c = S/4S_e f^2$. At the planning stage, data and hence the selected band is not available and so one may not be able to use (26) to assess Λ. Instead, one may take $N = \min(2\sqrt{J_c}, N_{max})$ to reflect that the usable bandwidth increases with s/n ratio J_0 up to a limit N_{max} set to control modelling error against, e.g., existence of unaccounted modes and assumption of locally flat modal force PSDs and noise PSDs. Equation (29) can be rewritten to give the required data duration (as a multiple of natural period):

$$\frac{1}{\frac{1}{2}\frac{1}{2^2}} \quad , \quad ^2 \quad , \quad ^2$$

'optimistic' min. req. duration

inflation due to finite s/n ratio

inflation due to finite bandwidth

Q_J 2 will allow for | A| up to 0.7. Remarkably, taking Q_J 1.25 (only 25% inflation) is sufficient to allow for | A| up 0.5, essentially because the bounding curve in Figure 5 is flat for small | A|. See Table 3 and Parts (e) and (f) of Figures 14, 16, 18 and 20 that report the statistics of | A| in some field tests. On the other hand, the factor $(1 \quad \sigma^2)(1 \ | \ A|^2)$ in the s/n ratio $\mathcal{M}$m

The mathematical theory for the uncertainty law of close modes is much more complicated than that for well-

$$R_{f_i} \quad d(1 \quad q_2^2 \mid A_1^2)^2 \cos^2(\quad s_i \quad f_i) \quad (1 \mid A_1^2)^2 q_2^2 \sin^2(\quad s_i \quad f_i \quad) \\ 2 \mid q_1 \mid\mid A_1^2 (1 \quad q_2^2 \mid A_1^2)(1 \mid A_1^2) q_2 \mid \cos(\quad s_i \quad f_i) \sin(\quad s_i \quad f_i \quad) \mid \tag{35}$$

Overestimating $|q_1|$ by q_2, the sines and cosines by 1, and simplifying gives the upper bound in (19). The lower and upper bounds of R_{f_i} can be attained by setting $f_1 \quad f_2$ and additionally

[8] Wenzel H, Pichler D (2005) Ambient Vibration Monitoring. John Wiley & Sons, UK

[9] R. Brincker, C. Ventura, Introduction to operational modal analysis, Wiley, London, 2015.

[10] S.K. Au, Operational Modal Analysis: Modelling, Inference, Uncertainty Laws. Springer, Singapore, 2017.

[11] C.Y. Shih, Y.G. Tsuei, R.J. Allemang, D.L. Brown, Complex mode indication function and its application to spatial domain parameter estimation, Mechanical Systems and Signal Processing, 2(4) (1988) 367-377.

[12] S.K. Au, F.L. Zhang, P. To, Field observations on modal properties of two tall buildings under strong wind, Journal of Wind Engineering and Industrial Aerodynamics, 101 (2012) 12-23.

[13] F.L. Zhang, C.E. Ventura, H.B. Xiong, W.S. Lu, Y.X. Pan, J.X. Cao, Evaluation of the dynamic characteristics of a super tall building using data from ambient vibration and shake table tests by a Bayesian approach, Structural Control and Health Monitoring, 25(4) (2017) e2121.

[14] M.J. Glanville, K.C.S. Kwok, Dynamic characteristics and wind induced response of a steel frame tower, Journal of Wind Engineering and Industrial Aerodynamics, 54–55 (1995) 133-149.

[15] A.P. Jeary, Damping measurements from the dynamic behaviour of several large multi-flue chimneys, Proceedings of the Institution of Civil Engineers, 57(2) (1974) 321-329.

[16] J.M.W. Brownjohn, E.P. Carden, C.R. Goddard, G. Oudin, Real-time performance monitoring of tuned mass damper system for a 183 m reinforced concrete chimney, Journal of Wind Engineering and Industrial Aerodynamics, 98(3) (2010) 169-179.

[17] A. DeVivo, C. Brutti, J.L. Leofanti, Modal shape identification of large structure exposed to wind excitation by operational modal analysis technique, Mechanical Systems and Signal Processing, 32(1-2) (2013) 195-206.

[18] J.M.W Brownjohn, A. Raby, J. Bassitt, A. Antonini, E. Hudson, P. Dobson, Experimental modal analysis of British rock lighthouses, Marine Structures, 62 (2018) 1-22.

[19] J.M.W. Brownjohn, F. Magalhaes, E. Caetano, A. Cunha, Ambient vibration re-testing and operational modal analysis of the Humber Bridge, Engineering Structures, 32(8) (2010) 2003-2018.

[20] A. Der Kiureghian, Structural Response to Stationary Excitation, Journal of the Engineering Mechanics Division 106 (1980) 1195–1213.

[21] A. Der Kiureghian, A response spectrum method for random vibration analysis of mdf systems,

[23]W.

of Sound and Vibration, 303(3–5) (2007) 475–500.

[37] Y.C. Zhu, S.K. Au, S. Jones, Uncertainty of Closely-Spaced Modes in Bayesian Modal